Journal of Metals, Materials and Minerals, 36(4), e2722, 2026

α-Fe_2O_3@MWCNT nanocomposite-based chemiresistive sensor for room temperature ethanol detection

Gayatri MOHAPATRA[1], Sabita TRIPATHY[1], Jyoti SHUKLA[2], Sunit Gourav MOHANTY[3], and Manoj Kumar DEBNATH[1,*]

[1] *Department of Electrical Engineering, Siksha O Anushandhan (deemed to be University), Bhubaneswar 751030, India*
[2] *Department of Electrical Engineering, SKIT M&G, Jaipur, Rajasthan,India*
[3] *Department of Environmental Sciences, Sambalpur University, Burla 768019, India*

***Corresponding author e-mail**: mkd.odisha@gmail.com

Received date:
22 April 2026
Revised date:
9 May 2026
Accepted date:
1 June 2026

Keywords:
Ethanol;
Fe_2O_3@MWCNT;
LIG;
Spray coating

Abstract

The development of low-cost nanostructured materials is vital to advancing the commercialization of sensors. In this study, α-Fe_2O_3@MWCNT nanocomposites were synthesized via a sustainable co-preparation approach, in which α-Fe_2O_3 was derived from readily available rusted iron, followed by calcination and subsequent mixing with multiwall carbon nanotubes (MWCNTs) to form a uniform sensing ink. The structural properties of the synthesized material were analyzed using X-ray diffraction (XRD) and scanning electron microscopy (SEM). The α-Fe_2O_3@MWCNT ink was then deposited onto laser-induced graphene electrodes for gas-sensing evaluation towards ethanol. The fabricated sensor exhibited a remarkable response and excellent selectivity toward ethanol at room temperature, displaying a response (R_{gas}/R_{air}) of 1.35, a response time of 98 s, and a recovery time of 70 s at 100 ppm. The enhanced sensing performance and cost-effective synthesis demonstrate the promise of rust-derived α-Fe_2O_3@MWCNT composites for real-time ethanol monitoring in different applications.

1. Introduction

The growing demand for low-cost, energy-efficient, and reliable chemical sensors has accelerated research into nanostructured materials with high surface activity and tunable chemical properties [1-6]. Among various detection technologies, metal oxide semiconductor (MOS) sensors have attracted considerable attention due to their simple design, low power consumption, and compatibility with miniaturized platforms [7-10]. Ethanol detection is of significant interest due to its extensive use in the fuel industry, food processing, hygiene products, and forensic applications. Monitoring ethanol in air is therefore essential for workplace safety, environmental control, and public health. However, achieving high sensitivity and selectivity at room temperature remains a major challenge for conventional MOS-based sensors, which often require high operating temperatures, resulting in higher power consumption and reduced long-term stability [11-18].

Iron oxide (Fe_2O_3) is a promising candidate for gas sensing because of low-cost, environmentally safe, abundant, and possesses excellent chemical stability, strong adsorption capacity, and rich redox activity. However, the low electrical conductivity and slow surface reactions of α-Fe_2O_3 can reduce its ability to detect effectively, particularly at room temperature (RT). To overcome these drawbacks, composite strategies that integrate conductive carbon-based materials have proven highly effective [1,19-22]. Multi wall carbon nanotubes (MWCNTs), with their remarkable electrical conductivity, high aspect ratio, and excellent mechanical strength, provide efficient electron transport pathways and improve the surface area for gas adsorption. Incorporating α-Fe_2O_3 nanoparticles into MWCNTs enhances charge-transfer efficiency and promotes synergistic interactions between the semi-conducting oxide and the conductive carbon network, thereby improving response and recovery characteristics toward volatile organic compounds (VOCs) such as ethanol [11,14,23,24].

Another critical factor in sensor fabrication is the synthesis approach. Conventional α-Fe_2O_3 preparation methods often involve chemical precursors, surfactants, or multi-step thermal treatments, which increase cost and environmental burden. In this study, a sustainable co-preparation route was developed to synthesize α-Fe_2O_3 from naturally occurring rusted iron, an abundant waste product. The rust-derived α-Fe_2O_3 was obtained through simple calcination, eliminating the need for sophisticated precursors or hazardous reagents. The low-cost oxide product was combined with MWCNTs to form α-Fe_2O_3@MWCNT nanocomposites, which were dispersed into a stable ink formulation suitable for direct deposition onto sensing substrates. This eco-friendly approach not only reduces material costs but also encourages the recycling of metal waste, making it very appealing for large-scale sensor production.

The fabricated α-Fe_2O_3@MWCNT ink was deposited onto laser-induced graphene (LIG) interdigitated electrodes, chosen for their high conductivity, porous structure, and facile fabrication. The LIG substrate provides a suitable surface for the uniform distribution of the composite and enables highly effective electron flow during sensing. When exposed to ethanol vapor at RT, the α-Fe_2O_3@MWCNT-based sensor exhibited a rapid, reversible response, demonstrating strong selectivity and

stability. This enhanced performance can be attributed to the synergistic interaction between α-Fe_2O_3 and MWCNTs, which enables efficient charge transfer and provides abundant active sites for ethanol adsorption and oxidation. The results confirm that the rust-derived α-Fe_2O_3@MWCNT sensor presents a cost-effective, sustainable, and high-performance solution for continuous ethanol monitoring in industrial and environmental applications.

2. Materials and methods

2.1 Materials

Rusted iron screws were utilized as a source of Fe, while all other chemicals were of analytical grade. Nitric acid (HNO_3, 69%, Sigma-Aldrich), hydrochloric acid (HCl, 37%, Sigma-Aldrich), and sodium hydroxide (NaOH, >97%, Fisher Chemical) were employed during the synthesis process. Polyvinylpyrrolidone (PVP) served as both a binder and a stabilizer during the preparation of the composite ink. Ethanol (EtOH) and isopropanol (IPA) of laboratory grade were acquired from Fisher Scientific (USA), and deionized (DI) water was produced using the in-house purification setup

2.2 Materials fabrication

Hematite (α-Fe_2O_3) was synthesized by thermal decomposition of rusted waste iron screw [1], while MWCNTs were functionalized using the method described by Belal *et al.* [11]. The LIG-IDE design consisted of six interdigitated fingers with 0.5 mm spacing and 0.5 mm finger width; the collection busbars on both sides were 1 mm wide [1] using a CO_2 laser engraver (VLS 4.6/75, Universal Laser Systems, 10.6 µm). The α-Fe_2O_3@MWCNT nanocomposite ink was formulated by dispersing 5 mg·mL^{-1} of the synthesized α-Fe_2O_3 and 0.2 mg·mL^{-1} functionalized MWCNTs (FMWCNTs) in EtOH with a ratio of α-Fe_2O_3 to MWCNT of 1:0.04. Polyvinylpyrrolidone (PVP, 2 mg·mL^{-1}) was included to improve the ink's dispersion stability and adhesion properties. The total solid loading was maintained at 5.2 mg·mL^{-1}, and the suspension was ultrasonicated for 10 min to obtain a uniform mixture. The resulting 150 µL of ink was then spray-deposited onto an LIG-IDE substrate (5 mm × 5.5 mm active area) with a mass loading of approximately 0.78 mg. During deposition, the spray nozzle was positioned 5 cm above the substrate, and compressed air at 20 PSI was used to ensure even coating. The coated films were annealed at 70°C for 1 h to remove residual solvents and moisture, thereby forming a stable, well-adhered α-Fe_2O_3@MWCNT sensing layer.

2.3 Characterization

The crystalline structure of the α-Fe_2O_3@MWCNT heteronanostructures was examined using X-ray diffraction (XRD; Rigaku Mini Flex 600, Japan) with Cu Kα radiation (λ = 1.5405 Å), operated at 40 kV and 35 mA. The surface morphology and structural features were characterized using a field-emission scanning electron microscope (FE-SEM, SU-8230, Japan). Gas-sensing measurements were carried out using the setup illustrated in Figure 1, designed to evaluate the sensor response toward VOCs at a controlled temperature of 30 ± 3°C. The sensing device was interfaced with a Keithley 2400c source meter (USA) for real-time electrical characterization. The experimental configuration comprised a sealed test chamber positioned on a hot plate, with airflow and temperature regulated by an integrated meter and fan to ensure homogenous gas distribution. The chamber also included humidity and temperature sensors to maintain ambient conditions of 10 RH% and 30 ± 3°C throughout the measurement. Ethanol vapor was generated by injecting a known volume of high-purity ethanol (99.99%) into the chamber through a micropipette, where the required volume (V) was calculated based on the target gas concentration (ppm) and chamber volume, as described by Equation (1) [25]. The sensor's response (SR) was determined using Equation (2) [26–28], derived from the ratio of resistance in ethanol exposure (R_{gas}) to the resistance of the sensor in air (R_{air}). The response time was defined as the time required for the resistance to reach 90% of its maximum change upon exposure to ethanol, while the recovery time was defined as the time required to return to 90% of the baseline resistance after reintroducing air [27,29,30].

$$V = \frac{Cv_a M}{2.46 \times 10^7 \times D} \quad (1)$$

Reducing gases and P type behaviour

$$SR = \frac{R_g}{R_a} \quad (2)$$

Here, C and v_a represent the target gas concentration (ppm) and the test chamber volume (mL), respectively, while M and D are the molecular weight (g·mol^{-1}) and density (g·mol^{-1}) of the ethanol.

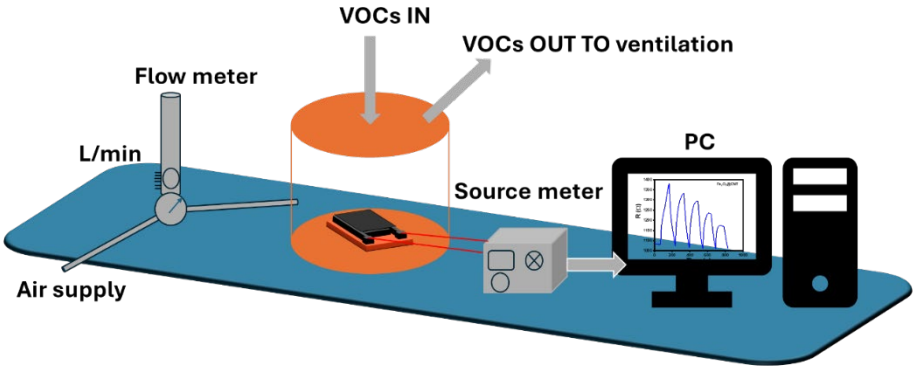

Figure 1. Schematic diagram of VOCs gas setup.

3. Results and discussion

3.1 Structural analysis

The XRD pattern of the α-Fe_2O_3@MWCNT heteronanostructures shows the coexistence of diffraction features from both MWCNTs show in Figure 2. A broad diffraction hump centered in the 20° to 30° range can be assigned to the (002) plane of graphitic MWCNTs, indicating the presence of a turbostratically disordered carbon framework. Superimposed on this background, several distinct diffraction peaks indexed to the (012), (104), (110), (113), (024), and (116) planes are observed, which are characteristic of crystalline α-Fe_2O_3, confirming the successful formation of iron oxide with well-defined lattice planes. The simultaneous observation of the MWCNT-related (002) reflection and multiple α-Fe_2O_3 reflections demonstrates the successful integration of α-Fe_2O_3 nanoparticles into the MWCNT matrix, forming a heteronanostructure in which the MWCNTs provide conductive support while the crystalline α-Fe_2O_3 domains are expected to serve as active sites for subsequent electro-chemical or sensing applications.

The SEM and EDS analysis depict α-Fe_2O_3@MWCNT thin film reveal a porous, fibrous morphology of intertwined MWCNT networks decorated with aggregated α-Fe_2O_3 nanoparticles (~20 nm to 50 nm), providing a high surface area for enhanced gas adsorption or electro-chemical activity, Figure 3. Elemental mapping shows homogeneous dispersion of Fe, O, C related to MWCNTs and trace N, confirming successful anchoring of hematite (α-Fe_2O_3) nanocrystals onto functionalized MWCNTs via chemical bonding (Fe-O-C interfaces), which prevents aggregation and improves electrical conductivity. The EDS spectrum quantifies dominant Fe and O peaks alongside C and N, indicating a metal oxide-carbon hybrid ideal for applications like gas sensing, where MWCNTs act as conductive scaffolds, enhancing charge transfer and sensitivity to analytes via Fe_2O_3's catalytic redox properties. Table 1 confirms the elemental weight and atomic percentages in α-Fe_2O_3@MWCNT.

3.2 VOCs sensing measurements

The gas-sensing characteristics of the sensor were evaluated using a 150 µL ink deposition patterned in a square geometry on the LIG-IDE substrate for ethanol detection. Figure 4 presents the comparative ethanol-sensing performance of the α-Fe_2O_3@MWCNT sensors when sequentially exposed to ethanol concentrations ranging from 20 ppm to 100 ppm in dry air (RH = 10%) at 30 ± 3°C. The sensor exhibited a typical *p*-type response toward ethanol, demonstrating an increase in resistance during a 90 s exposure to the reducing gas, attributed to electron donation from ethanol molecules to the sensing layer. At 100 ppm ethanol, the α-Fe_2O_3@MWCNT device achieved a high response (Rgas/Rair) of 1.35, with rapid response and recovery times of 98 s and 70 s, respectively, as shown in Figure 4(a-b).

As shown in Figure 4(c-d), the sensor exhibits strong selectivity for ethanol compared to isopropanol (IPA) and acetone at 100 ppm, which is crucial for reliable real-time gas discrimination with high precision and response. In the α-Fe_2O_3@MWCNT composite system, this selectivity originates from the formation of a p–n heterojunction at the interface between *n*-type α-Fe_2O_3 and *p*-type MWCNTs. The heterojunction modulates charge-carrier dynamics and resistance depending on the target gas, thereby influencing sensing behavior [31]. Figure 4(e-f) further demonstrates the sensor's cyclic stability toward 100 ppm ethanol over five consecutive cycles, displaying an average response of 1.35. Each exposure cycle results in a reproducible decrease in resistance, followed by a complete recovery upon gas removal, confirming excellent reversibility and surface regeneration. Additionally, Figure 5 comprehensively evaluates the electrical, structural, and operational robustness of the fabricated gas-sensing platform under diverse testing parameters. Long-term stability testing (Figure 5(a)) shows consistent sensor performance over 14 days, validating its capability for durable, reliable ethanol detection. The device's potential for flexible electronics is examined via impedance analyzer in (Figure 5(b)), which reveals the frequency-dependent impedance (Z) profiles under varying mechanical strain profiles, including flat, 30°, and 50° bending configurations, where the minimal deviation in impedance response highlights the structural integrity of the composite on the substrate under mechanical deformation. Furthermore, the high reproducibility of the fabrication methodology is validated in (Figure 5(c)), showing highly uniform performance characteristics. Finally, the electronic junction dynamics and ohmic contact characteristics are analyzed through current-voltage sweeps spanning from 0 V to 5 V (Figure 5(d-e)).

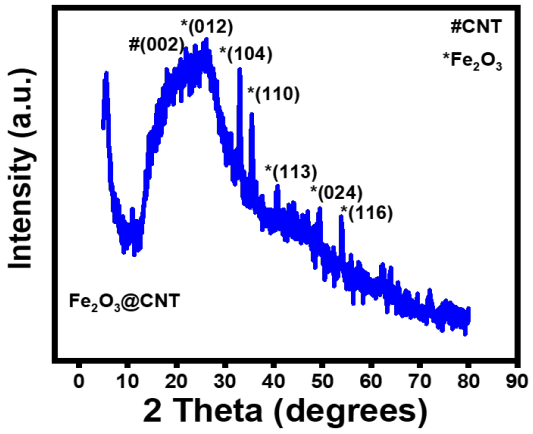

Figure 2. XRD pattern of α-Fe_2O_3@MWCNT heteronanostructures.

Table 1 EDS Mapping Elemental Composition.

Materials	Element	wt%	Atomic [%]
α-Fe_2O_3@MWCNT	C	26.63	46.93
	N	2.06	3.11
	O	24.28	32.13
	Fe	47.03	17.83
	Total	100.00	100.00

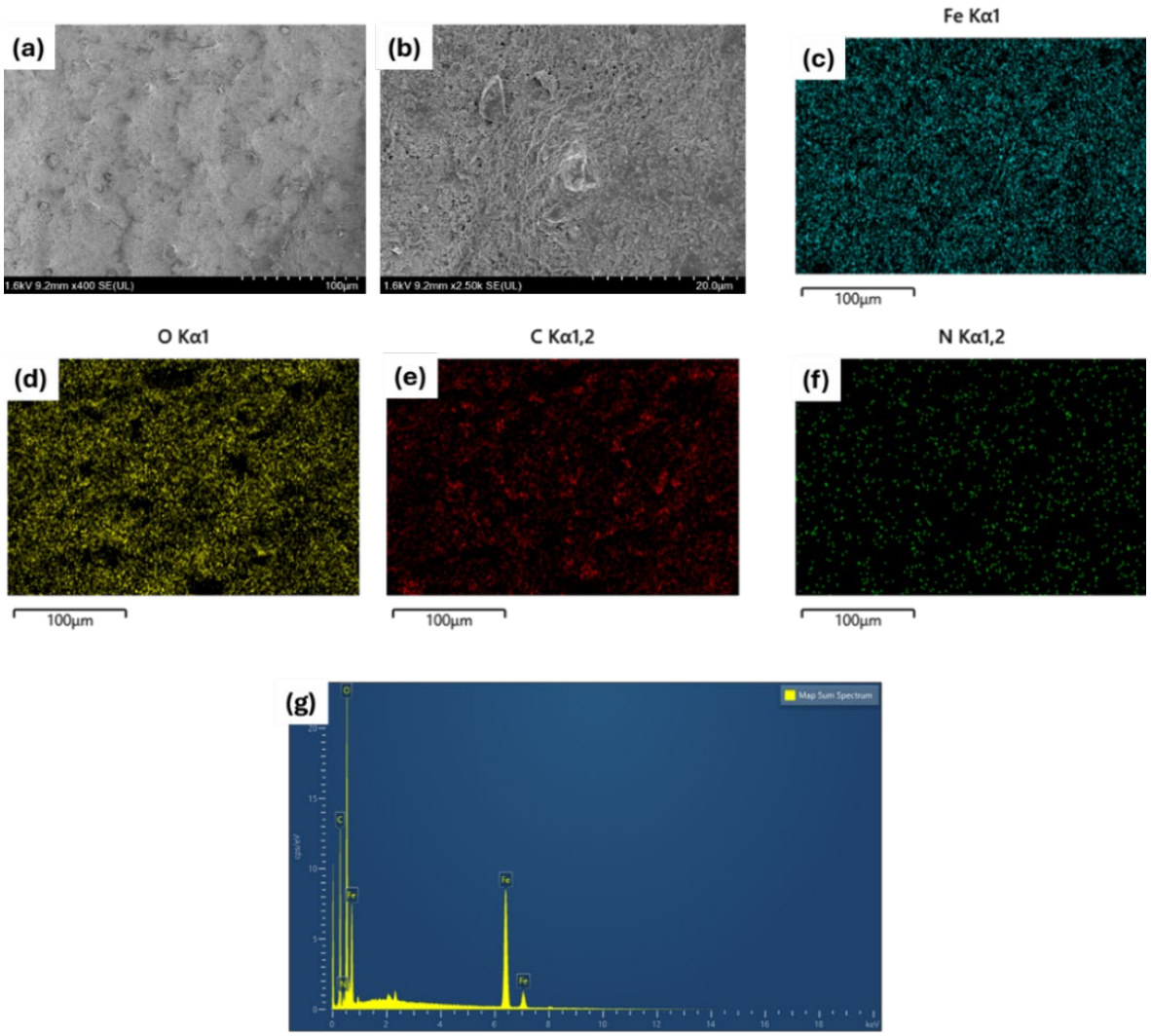

Figure 3. SEM images and EDS of (a-b) α-Fe_2O_3@MWCNT films; (c-g) α-Fe_2O_3@MWCNT EDs.

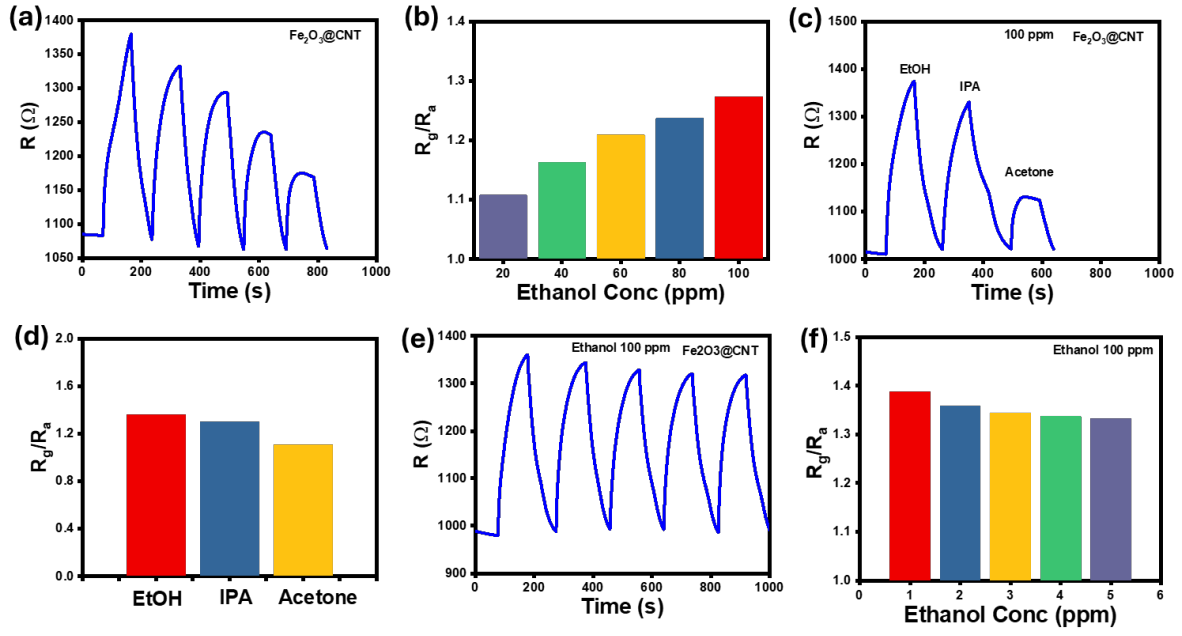

Figure 4. Gas sensing performance of α-Fe_2O_3@MWCNT towards EtOH at RT: (a-b) Gas sensing performance at different concentrations from 100 ppm to 20 ppm; (c-d) Selectivity towards ethanol, IPA, and acetone at 100 ppm; and (e-f) Cyclic stability at 100 ppm of ethanol.

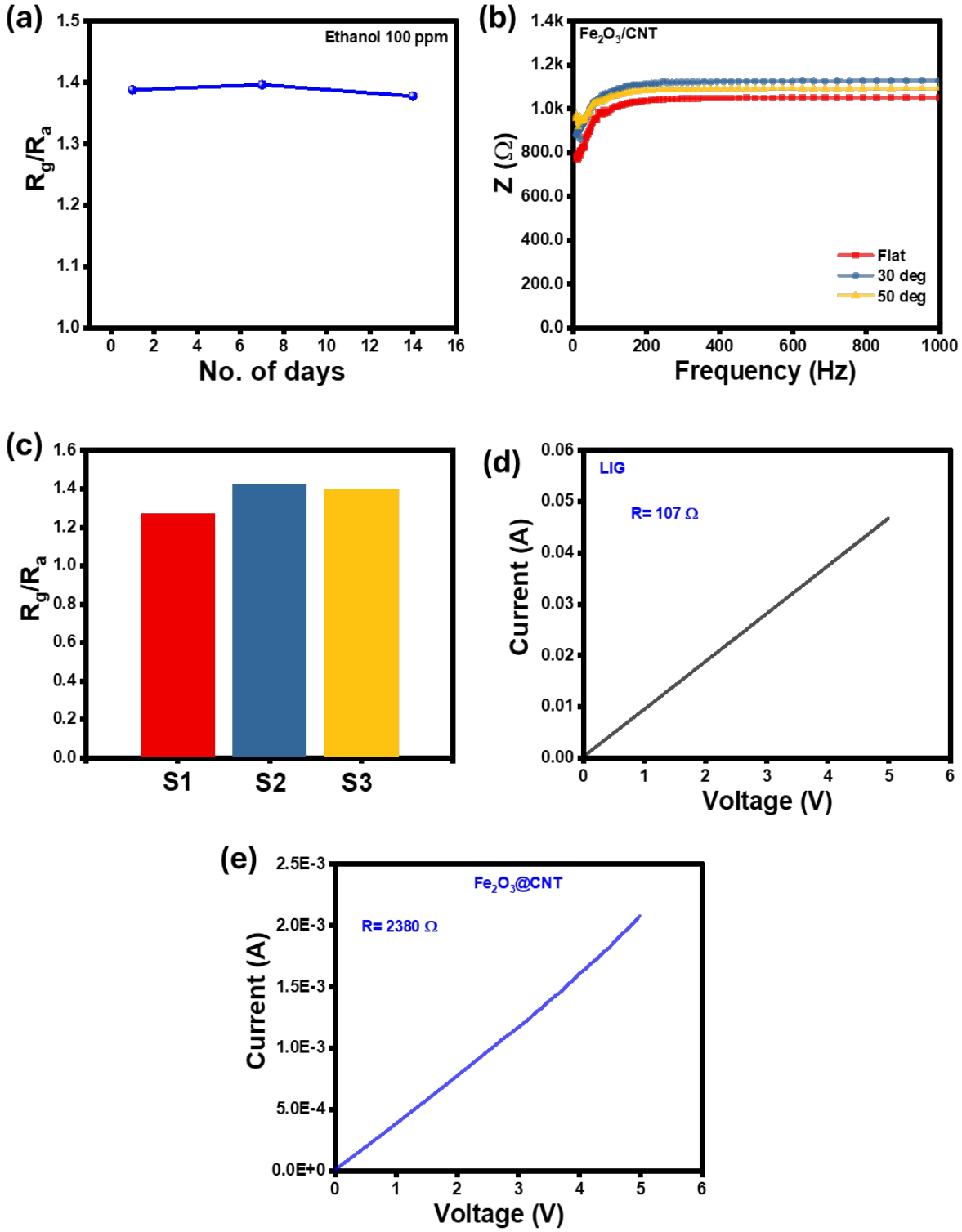

Figure 5. (a) Lifetime stability of α-Fe_2O_3@MWCNT towards EtOH at RT and 100 ppm, (b) Impedance spectroscopy analysis at different bending angles, (c) Reproducibility test, (d) Current-voltage of LIG, (e) Current-voltage of α-Fe_2O_3@MWCNT.

Table 2 summarizes recent studies from the literature for comparison, while Figure 6 illustrates the proposed ethanol-sensing mechanism. The sensing process is governed by the redox interactions between ethanol molecules and chemisorbed oxygen species (such as O^- and O_2^-) on the sensor surface [32,33]. When ethanol is introduced, it reacts with the adsorbed oxygen ions, releasing electrons into the conduction band and thereby reducing the sensor's resistance. This mechanism underscores effective electron transfer and strong redox coupling between ethanol and surface oxygen species, thereby decreasing the extent of the electron-depletion layer (EDL).

$$C_2H_5OH\ (\text{gas}) \rightarrow C_2H_5OH\ (\text{ads}) \quad (3)$$

$$C_2H_5OH\ (\text{ads}) + 3O_2^-\ (\text{ads}) \rightarrow 2CO_2 + 3H_2O + 3e^- \quad (4)$$

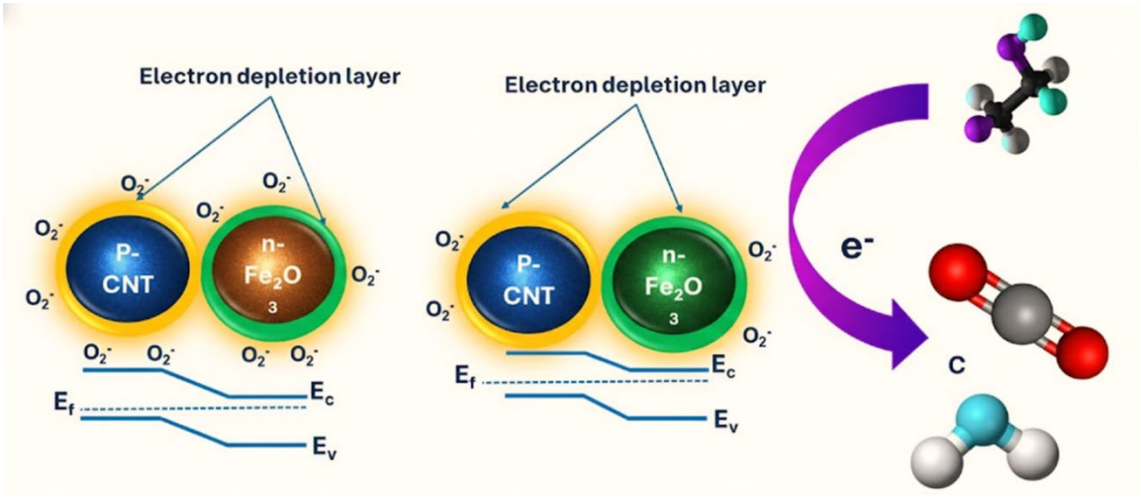

Figure 6. Gas sensing mechanism.

Table 2. EtOH ethanol sensing performance compared to reported works in literature.

Materials	EtOH [ppm]	Temp [°C]	Response $s_1 = (\Delta R/R_a) \times 100\%$ or $s_2 = R_g/R_a$ or R_a/R_g	Response/ Recovery time [s]	Ref.
Fe_2O_3@CNT	100	RT	S_2=1.35 S_1= 35%	98/70	This Work
α-Fe_2O_3	100	RT	S_2=47.00	104/126	[1]
SnO_2	100	RT	S_2=7.5	61.5/104	[7]
SnO_2-CuO	100	RT	S_2=11	53/64	[7]
SnO_2	100	350	S_2=10.5	5/40	[34]
Fe_2O_3-Co_3O_4 composite	100	250	S_2=26.2	-/-	[35]
α-Fe_2O_3 nanoparticles	100	150	S_1=14.5	-/-	[36]
α-Fe_2O_3(0.09)/Nb_2O_5	100	160	S_2=12.6	8/2	[37]

4. Conclusions

This work reports a detailed investigation of α-Fe_2O_3@MWCNT nanostructured ethanol sensors fabricated via a sustainable microwave-assisted synthesis and subsequent thermal annealing. Comprehensive characterization using SEM, XRD, and gas-sensing analyses confirmed the successful formation of α-Fe_2O_3@MWCNT heterostructures with well-developed surface morphology and abundant oxygen-rich active sites, which facilitated efficient ethanol adsorption. The resulting sensors exhibited excellent room-temperature performance, featuring high selectivity, rapid response and recovery times, and stable long-term operation. Specifically, the α-Fe_2O_3@MWCNT device achieved a response of 1.35 with response and recovery times of 98 s and 70 s, respectively, at 100 ppm ethanol, underscoring its promise for practical low-temperature ethanol sensing applications.

References

[1] M. A. Belal, S. Hajra, A. M. Bayoumy, M. H. Eldesouki, K. R. Kaja, S. Panda, D. Ramu, A. A. El-moneim, P. G. R. Achary, and H. J. Kim, "Transformation of rusted iron into an IDE-based sensor for ethanol detection and self-powered humidity sensing," *Journal of Materiomics,* vol. 12, no. 4, p. 101188, 2026.

[2] A. M. Bayoumy, A. Hessein, M. A. Belal, M. Ezzat, M. A. Ibrahim, A. Osman, and A. A. El-Moneim, "Microdrop InkJet printed supercapacitors of graphene/graphene oxide ink for flexible electronics," *Journal of Power Sources,* vol. 617, p. 235145, 2024.

[3] M. A. Belal, S. Hajra, S. Panda, K. R. Kaja, A. A. El-Moneim, P. G. R. Achary, and H. J. Kim, "Mechanochemically synthesized ZIF-8@ ZnO composite-based NO_2 gas detection," *New Journal of Chemistry,* vol. 49, no. 42, pp. 18436-18446, 2025.

[4] S. A. Behera, S. Hajra, S. Panda, A. K. Sahu, P. Alagarsamy, Y. K. Mishra, H. J. Kim, and P. G. R. Achary, "Synergistic energy harvesting and humidity sensing with single electrode tribo-electric nanogenerator," *Ceramics International,* vol. 50, no. 19, pp. 37193-37200, 2024.

[5] S. A. Behera, S. Hajra, S. Panda, A. Amanat, and P. G. R. Achary, "Structural and electrical properties of 0.98($K_{0.5}Na_{0.5}NbO_3$)-0.02($Bi_{0.5}Na_{0.5}$)TiO_3 ceramics," *Journal of Metals, Materials and Minerals,* vol. 33, no. 4, 2023,

[6] M. Niharika, R. Garlapallya, K. Ruthvik, M. Velaga, and B. M. Rao, "Hydrogen production on g-C_3N_4 nanoflakes via photo-electrochemical water splitting," *Materials Today: Proceedings,* 2023.

[7] P. Chaiyo, M. A. Belal, S. Hajra, S. Panda, P. Bhosale, H. Keum, and H. J. Kim, "Low-cost domestic microwave synthesis of

SnO_2/CuO nanostructure for ethanol detection," *Micro and Nano Systems Letters,* vol. 13, no. 1, 2025

[8] M. A. Belal, S. Hajra, S. Panda, K. R. Kaja, M. Magdy, A. A. El Moneim, D. Janas, Y. K. Mishra, and H. J. Kim, "Advances in gas sensors using screen printing," *Journal of Materials Chemistry A,* vol. 13, no. 8, pp. 5447–5497, 2025.

[9] N. Kumar, Q.-V. Hoang, M. A. Belal, K. R. Kaja, P. H. Nguyen, Q. Le-Van, V. Vo, V. T. T. Linh, P. K. T. Nguyen, and Q. T. H. Ta, "Progress in synthesis of $Ti_3C_2T_x$ MXene-based nanostructures for energy harvesting and storage: A review," *Journal of Science: Advanced Materials and Devices,* vol. 10, no. 4, p. 101034, 2025.

[10] S. K. Chirauri, M. Rakshita, and D. Haranath, "An Insights into non-re doped materials for opto-electronic display applications," in *Emerging Materials: Design, Characterization and Applications*: Springer, 2022, pp. 433-472.

[11] M. A. Belal, S. Hajra, S. Panda, K. R. Kaja, K. J. Park, R. Jana, P. G. R. Achary, and H. J. Kim, "Functionalized MWCNTs@ ZnO nanocomposites via spray printing for NO_2 gas sensing," *Journal of Materials Science: Materials in Electronics,* vol. 36, no. 12, p. 750, 2025.

[12] J. Panda, M. A. Belal, H. J. Jung, J. Baek, S. Hajra, M. W. Pin, J. W. Park, S. Panda, V. Vivekananthan, J.-G. Yeo, S. S. Jang, H. J. Kim, and K, Y. Cho, "Defect-engineered activated bimetallic MOFs on laser-induced graphene for enhanced NO_2 sensing," *Journal of Environmental Chemical Engineering,* vol. 14, no. 1, p. 120484, 2025.

[13] P. C. Tagbo, A. M. Bayoumy, M. A. Belal, M. S. Nofal, M. M. Ayad, and A. Abd El-Moneim, "MoS_2-driven morphological evolution and defect engineering in ZnO nanoplates for enhanced room-temperature carbon monoxide sensing," *Microchemical Journal,* vol. 221, p. 116908, 2026.

[14] G. T. Taulo, A. E. Moharm, M. A. Belal, N. M. Shaalan, M. M. Ayad, G. G. Mohamed, and A. A. El-Moneim, "Impact of NS co-doped rGO on the CO gas sensing performance of inkjet-printed SnO_2 nanoparticles," *Sensors and Actuators B: Chemical,* vol. 443, p. 138186, 2025.

[15] S. A. Behera, H.-G. Kim, I. R. Jang, S. Hajra, S. Panda, N. Vittayakorn, H. J. Kim, and P. G. R. Achary, "Triboelectric nanogenerator for self-powered traffic monitoring," *Materials Science and Engineering: B,* vol. 303, p. 117277, 2024.

[16] S. A. Behera, A. Amanat, and P. G. R. Achary, "Photocatalytic degradation of ciprofloxacin drug utilizing novel PVDF/ polyaniline/lanthanum strontium manganate@Ag composites," *Journal of Metals, Materials and Minerals,* vol. 34, no. 1, 2024.

[17] M. H. Eldesouki, M. M. Mohamed, and A. Abdelmoniem, "Targeting hydrogen-rich gasoline production from CO_2 via a sustainable Fe-Cu tandem catalyst," *Journal of Environmental Chemical Engineering,* vol. 13, no. 3, 2025.

[18] A. Tyagi, M. Rakshita, D. Haranath, and C. Shivakumara, "Thermally stable Li^+ co-doped $ZnMoO_4$: Eu^{3+} phosphors for white LEDs, nitroaromatic sensing and low temperature non-contact optical thermometry applications," *Materials Advances,* vol. 6, no. 16, pp. 5758–5776, 2025.

[19] M. H. Eldesouki, M. M. Mohamed, and A. Abd El-Moneim, "Semi-industrial CO and CO_2 conversion with biochar-supported Fe-based catalysts," *Carbon Resources Conversion,* p. 100358, 2025.

[20] A. G. Galallah, M. K. Albolkany, A. E. Rashed, W. Sadik, A.-G. El-Demerdash, and A. Abd El-Moneim, "Optimizing Mo_2C-based catalytic system for efficient CO_2 conversion and CO selectivity through carbon-nitrogen supporting and potassium promotion," *Journal of Environmental Chemical Engineering,* vol. 12, no. 5, p. 113380, 2024.

[21] J. A. L. Jayarathna, and K. R. Kaja, "Energy-harvesting device based on lead-free perovskite," *AI, Computer Science and Robotics Technology,* vol. 3, no. 1, pp. 1–9, 2024.

[22] A. A. Sharma, P. P. Pradhan, K. D. Prasad, M. Rakshita, R. Pembarthi, and D. Haranath, "Multimodal luminescence and energy transfer mechanism in a narrowband UVB emitting phosphor system towards futuristic phototherapeutic devices," *Materials Advances,* vol. 6, no. 22, pp. 8400–8413, 2025.

[23] M. A. Belal, S. Hajra, S. Panda, K. R. Kaja, K. J. Park, and H. J. Kim, "Spray-printed ZnO thin film for high-sensitivity NO_2 gas sensing," *Micro and Nano Systems Letters,* vol. 13, no. 1, 2025.

[24] S. Nuthalapati, A. Chakraborthy, I. Arief, K. Meena, K. R. Kaja, R. R. Kumar, U. K. Khanapuram, A. Das, M. E. Lltinsoy, and A. Nag, "Wearable high-performance MWCNTs/PDMS nano-composite-based triboelectric nanogenerators for haptic applications," *IEEE Journal on Flexible Electronics,* vol. 3, no. 9, pp. 393–400, 2024.

[25] R. T. Parayil, B. Bhagat, S. K. Gupta, K. Mukherjee, and M. Mohapatra, "Oxygen vacancy-enriched Zn_2SnO_4 for aliphatic alcohol sensing and enhanced selectivity towards n-butanol," *Physical Chemistry Chemical Physics,* vol. 26, no. 9, pp. 7424–7434, 2024.

[26] S. N. Birajdar, and P. V. Adhyapak, "Palladium-decorated vanadium pentoxide as NO_x gas sensor," (in English), *Ceramics International,* vol. 46, no. 17, pp. 27381–27393, 2020.

[27] D. M. ME, N. G. Sundaram, A. Singh, A. K. Singh, and S. B. Kalidindi, "An amine functionalized zirconium metal-organic framework as an effective chemiresistive sensor for acidic gases," *Chemical communications (Cambridge, England),* vol. 55, no. 3, pp. 349–352, 2019.

[28] X. L. Liu, S.-X. Ma, S.-W. Zhu, Y. Zhao, X.-J. Ning, L. Zhao, and J. Zhuang, "Light stimulated and regulated gas sensing ability for ammonia using sulfur-hyperdoped silicon," (in English), *Sensors and Actuators B: Chemical,* vol. 291, pp. 345–353, 2019.

[29] J. Y. Park, Y. Kwak, Y.-R. Lim, S.-W. Park, M. S. Lim, H.-B. Cho, N. V. Myung, and Y.-H. Choa, "Tuning the sensing responses towards room-temperature hypersensitive methanol gas sensor using exfoliated graphene-enhanced ZnO quantum dot nano-structures," *Journal of Hazardous Materials,* vol. 438, p. 129412, 2022.

[30] J. Jaiswal, P. Singh, and R. Chandra, "Low-temperature highly selective and sensitive NO_2 gas sensors using CdTe-functionalized ZnO filled porous Si hybrid hierarchical nanostructured thin films," *Sensors and Actuators B: Chemical,* vol. 327, p. 128862, 2021.

[31] S. M. Ingole, A. C. Molane, U. J. Patel, S. L. Patil. M. Selvaraj, M. A. Assiri, P. A. Mahanwar, and V. B. Patil, "Development of

SnO_2/CuO heterostructure sensor for detection of toxic NO_2 gas," *Inorganic Chemistry Communications,* vol. 182, p. 115402, 2025,

[32] P. C. Tagbo, M. M. Mohamed, M. M. Ayad, and A. Abd El-Moniem, "Fabrication of flexible MoS_2 sensors for high-performance detection of ethanol vapor at room temperature," (in English), *Sensor Actuat a-Phys,* vol. 389, p. 116531, 2025.

[33] A. Thomas, L. Thirumalaisamy, S. Madanagurusamy, and K. Sivaperuman, "Incompatibility of pure SnO_2 thin films for room-temperature gas sensing application," *ACS Omega,* vol. 8, no. 36, pp. 32848–32854, 2023.

[34] B. Wang, L. Sun, and Y. Wang, "Template-free synthesis of nanosheets-assembled SnO_2 hollow spheres for enhanced ethanol gas sensing," (in English), *Materials Letters,* vol. 218, pp. 290–294, 2018.

[35] S. M. H. B. Enferadi, and A. Mirzaei, "Fe_2O_3-Co_3O_4 nano-composite gas sensor for ethanol sensing studies," *Ceramic International,* vol. 50, no. 24, pp. 52861–52870, 2024.

[36] M. Shoorangiz, L. Shariatifard, H. Roshan, and A. Mirzaei, "Selective ethanol sensor based on α-Fe_2O_3 nanoparticles," (in English), *Inorganic Chemistry Communications,* vol. 133, p. 108961, 2021.

[37] R. Khatoon, S. R.auf, M. U. Haq, S. Attique, S. U. Din, N. Ali, Y. Guo, H. Chen, Y. Tian, and J. Lu, "Design of highly sensitive and selective ethanol sensor based on alpha-Fe_2O_3/Nb_2O_5 hetero-structure," *Nanotechnology,* vol. 32, no. 19, p. 195503, 2021.